JOURNAL OF TISSUE ENGINEERING AND REGENERATIVE MEDICINE
J Tissue Eng Regen Med 2016; **10**: 748–761.
Published online 27 December 2013 in Wiley Online Library (wileyonlinelibrary.com) **DOI:** 10.1002/term.1834

RESEARCH ARTICLE

Abdominal wall reconstruction by a regionally distinct biocomposite of extracellular matrix digest and a biodegradable elastomer

Keisuke Takanari[1,2†,#], Yi Hong[1,2‡,#], Ryotaro Hashizume[1,2§], Alexander Huber[1,2], Nicholas J. Amoroso[1,3], Antonio D'Amore[1,3,4,5], Stephen F. Badylak[1,2,3] and William R. Wagner[1,2,3,6*]

[1]*University of Pittsburgh, McGowan Institute for Regenerative Medicine, Pittsburgh, PA, USA*
[2]*University of Pittsburgh, Department of Surgery, Pittsburgh, PA, USA*
[3]*University of Pittsburgh, Department of Bioengineering, Pittsburgh, PA, USA*
[4]*RiMED Foundation, Palermo, Italy*
[5]*DICGIM University of Palermo, Palermo, Italy*
[6]*University of Pittsburgh, Department of Chemical Engineering, Pittsburgh, PA, USA*

Abstract

Current extracellular matrix (ECM) derived scaffolds offer promising regenerative responses in many settings, however in some applications there may be a desire for more robust and long lasting mechanical properties. A biohybrid composite material that offers both strength and bioactivity for optimal healing towards native tissue behavior may offer a solution to this problem. A regionally distinct biocomposite scaffold composed of a biodegradable elastomer (poly(ester urethane)urea) and porcine dermal ECM gel was generated to meet this need by a concurrent polymer electrospinning/ECM gel electrospraying technique where the electrosprayed component was varied temporally during the processing. A sandwich structure was achieved with polymer fiber rich upper and lower layers for structural support and an ECM-rich inner layer to encourage cell ingrowth. Increasing the upper and lower layer fiber content predictably increased tensile strength. In a rat full thickness abdominal wall defect model, the sandwich scaffold design maintained its thickness whereas control biohybrid scaffolds lacking the upper and lower fiber-rich regions failed at 8 weeks. Sandwich scaffold implants also showed higher collagen content 4 and 8 weeks after implantation, exhibited an increased M2 macrophage phenotype response at later times and developed biaxial mechanical properties better approximating native tissue. By employing a processing approach that creates a sheet-form scaffold with regionally distinct zones, it was possible to improve biological outcomes in body wall repair and provide the means for further tuning scaffold mechanical parameters when targeting other applications. Copyright © 2013 John Wiley & Sons, Ltd.

Received 13 November 2012; Revised 19 May 2013; Accepted 2 September 2013

Keywords **abdominal wall reconstruction; extracellular matrix; biodegradable; elastomer; electrospinning; polyurethane; scaffold**

1. Introduction

Incisional hernia is a common complication after abdominal surgery with an occurrence rate estimated to be 10–20% (Mudge and Hughes, 1985; den Hartog *et al*., 2008; Cassar and Munro, 2002). Approximately 115 000 ventral hernia or abdominal wall defects repairs are performed in the USA with recurrence (30–50%) associated with infection or multiple previous surgeries (van der Linden and van Vroonhoven, 1988; den Hartog

Correspondence to: W. R. Wagner, McGowan Institute for Regenerative Medicine, University of Pittsburgh, Pittsburgh, PA, USA.
E-mail: wagnerwr@upmc.edu
[†]*Present address: Nagoya University, Department of Plastic and Reconstructive Surgery, Nagoya, Aichi, Japan.*
[‡]*Present address: University of Texas at Arlington, Department of Bioengineering, Arlington, TX, USA.*
[§]*Present address: Mie University Graduate School of Medicine, Department of Pathology and Matrix Biology, Tsu, Mie, Japan.*
[#]*Both authors contributed equally to this work.*

et al., 2008). Various kinds of synthetic implants are used to repair incisional hernia and abdominal wall defects, including biodegradable and non-degradable mesh, however, there are limitations with these materials (van der Linden and van Vroonhoven, 1988; Cassar and Munro, 2002; Dumanian and Denham, 2003; den Hartog *et al*., 2008; Sanchez *et al*., 2011). For example, synthetic meshes should not be used in patients with previous wound infections, abdominal fistula or immunosuppression because of a high infection risk. In some clinical cases, non-degradable implants have to be removed after a period of implantation because of infection, protrusion or patient discomfort resulting from mechanical property mismatch between the native body wall and the synthetic material. An ideal situation, not currently achievable, would be to facilitate a healing response that creates mechanically functional native tissue, while avoiding mechanical failure during the period of tissue remodelling. While current biological scaffolds offer promising regenerative responses in many settings (Badylak *et al*., 2012), in some applications concerns arise with the maintenance of adequate mechanical properties.

The purpose of this study was to create and to evaluate *in vivo* a biohybrid composite material that offers both strength and bioactivity for optimal healing towards native tissue behaviour. Such a material would be applicable in a variety of fascial and/or muscle tissue reconstruction procedures. The model used in this study, a full wall thickness replacement, would have similarities to clinical scenarios where there is abdominal wall excision and loss due owing cancer, infection-related necrosis, trauma or to extremely large abdominal wall hernias where the rectus muscles are laterally displaced. Dermal extracellular matrix (dECM) gel possesses attractive biocompatibility and bioactivity, with weak mechanical properties and rapid degradation (Hodde *et al*., 2001; Hong *et al*., 2011; Reing *et al*., 2010), while conventionally electrospun biodegradable, elastomeric poly(ester urethane)urea (PEUU) has strong mechanical properties with controllable degradation rates, but elicits a proinflammatory host response (Hong *et al*., 2008, 2009; Stankus *et al*., 2008; Hashizume *et al*., 2010; Soletti *et al*., 2011). In previous work, the integration of dECM gel with PEUU was successfully performed utilizing a concurrent electrospinning/electrospraying method (Hashizume *et al*., 2010; Hong *et al*., 2011). The material showed a high degree of cellular infiltration when compared with synthetic material alone and had tensile mechanical properties that approximated those of the native abdominal wall tissue 4 weeks after rat abdominal wall implantation. However, as is demonstrated in this report, the material failed to maintain its mechanical strength at longer implantation times in the face of intra-abdominal pressure, with thinning and herniation being observed by 8 weeks.

In addition to this observation, a solution to this problem is reported through the development of a new approach to creating a biohybrid composite scaffold in which a material is generated with two polymer-rich mechanically supportive layers integrated on the upper and lower surfaces. These upper and lower fascia transition into a central layer comprising a dECM/polymer composite, where the dECM component putatively serves to encourage tissue integration. The idea of adding the supportive layers on the top and bottom of the scaffold was conceived from the role of fascia as a mechanical support to native muscle tissue. To evaluate the histological and mechanical remodelling of biocomposite scaffold designs with and without mechanically supportive elements a rat full-thickness abdominal wall replacement model was employed.

2. Materials and methods

2.1. dECM gel formation

Dermal ECM gel was prepared as described previously (Hong *et al*., 2011). Briefly, the epithelial layer and underlying connective tissue were resected from fresh porcine skin and the remaining dermis layer was processed to achieve decellularization. The resulting dermal matrix sheet was rinsed in deionized water, frozen and lyophilized. A powder was created from the lyophilized sheet using a Waring commercial blender and Wiley Mill. Particulate lyophilized matrix was then digested by 1 mg/ml pepsin in 0.01 N HCl. The suspension was mixed on a stir plate at room temperature for 48 h until no visible particulates remained. The resulting dECM digest (0.75 ml), 10× phosphate-buffered saline (PBS) (0.083 ml), 0.1 N NaOH (0.075 ml) and 1× PBS (0.092 ml) were mixed together on ice to make 1 ml of a 15 mg/ml gel, and used immediately afterwards for electrospraying.

2.2. Scaffold fabrication

An approach to creating a regionally distinct scaffold was employed where a dECM gel-rich layer was bordered by the two supportive polymer-rich outer layers using a concurrent electrospinning/electrospraying procedure (Hong *et al*., 2011; Hashizume *et al*., 2010) (Figure 1a). Poly(ester urethane) urea was synthesized from polycaprolactone diol (PCL, Mn = 2000; Sigma, St. Louis, MO, USA), 1,4-diisocyanatobutane (BDI; Sigma) and putrescine (Sigma) at a molar ratio of 1:2:1 PCL–BDI–putrescine according to the methods of previous reports (Guan *et al*., 2002; Stankus *et al*., 2008). For the two polymer-rich layers, PBS was fed by a syringe pump at 0.2 ml/min into a capillary (1.2 mm inner diameter) charged at 7 kV and suspended 4 cm above the target mandrel (19 mm diameter). Concurrently, PEUU in hexafluoroisopropanol solution (12%, w/v) was fed at 1.5 ml/h from a capillary, charged at 12 kV and perpendicularly located 20 cm from the target mandrel. The mandrel was charged at −4 kV and rotated at 250 rpm (8 cm/s tangential velocity) while translating back and forth 8 cm along the *x*-axis at 0.15 cm/s. For the dECM gel-rich layer, 10 ml dECM gel solution (15 mg/ml) was fed at 1.5 ml/min, and the

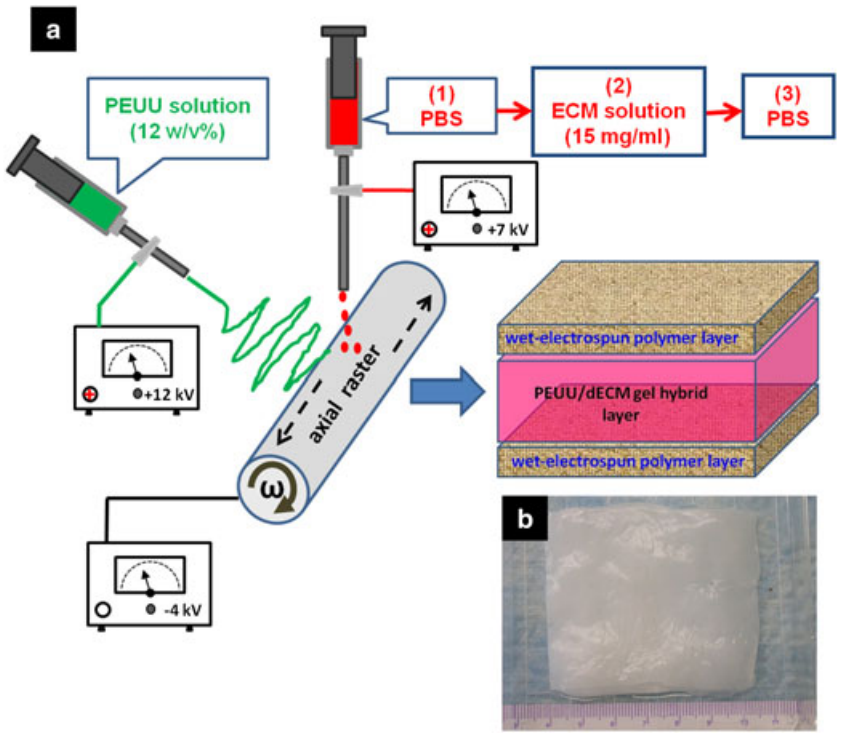

Figure 1. (a) Schematic of processing method for sandwich scaffold fabrication. Phosphate-buffered saline (PBS) or extracellular matrix (ECM) gel from one syringe (red) was electrosprayed while polymer solution in a separate syringe (green) was electrospun. To achieve the regionally distinct 'sandwich'-like structure, the processing stream from the electrospraying capillary proceeded in the following order over the course of scaffold generation: (1) PBS, (2) dermal extracellular matrix (dECM) gel solution, and (3) PBS. The time for the two PBS electrospraying periods were equivalent. PEUU, elastomeric poly(ester urethane)urea. (b) Gross appearance of the scaffold after gelation

PEUU solution infusion rate was changed to 20 ml/h, while other electrospinning parameters remained the same as for the polymer-rich layers. To achieve the regionally distinct 'sandwich'-like structure, the processing stream from the electrospraying capillary proceeded in the following order over the course of scaffold generation: (1) PBS, (2) dECM gel solution and (3) PBS. The wet electrospinning (polymer electrospinning + PBS electrospraying) time for the top and bottom layers was the same. A series of sandwich scaffolds were fabricated by altering the wet electrospinning time (10, 20, 30 min). The scaffolds formed were cut and removed from the mandrel and transferred to a 37 °C incubator for 45 min to allow the dECM to thermally gel.

To evaluate the benefit of utilizing the regionally distinct processing, control biohybrid scaffolds were generated that lacked the polymer-rich upper and lower layers. These were created by feeding 10 ml porcine dECM gel solution (15 mg/ml) at 1.5 ml/min for electrospraying, and a PEUU solution at 20 ml/h for electrospinning, while maintaining all other processing parameters as in the above description. Both scaffolds possessed similar thickness with no statistical difference between them (2.45 ± 0.09 mm for sandwich scaffolds).

2.3. Scaffold characterization

A macroscopic image of a sandwich sample was taken by a digital camera, and the scaffold cross-section morphology was observed under scanning electronic microscopy after cutting liquid nitrogen cooled samples that were then freeze-dried and sputter coated. Peak uniaxial tensile strength and strain in orthogonal directions were measured on an MTS Tytron 250 MicroForce Testing Workstation (Pittsburgh, PA, USA) according to ASTM D638-98 (ASTM International, West Conshohocken, PA, USA). Briefly, materials were sectioned into samples with dimensions of 5 mm x 25 mm. Samples were subjected to uniaxial tensile strain at a crosshead speed of 25 mm/min until mechanical failure. Four samples were tested for each scaffold type in each direction. Suture retention strength was tested with a BIOSYN UM-214 4–0 suture (Coviden, Dublin, Ireland) under the same conditions. A single suture loop was created 5 mm from the short edge (so as to pull in the longitudinal direction) and fixed on the upper clamp. Suture retention strength was calculated as suture load/(suture diameter × sample thickness) at the point of tearing. Four samples were used for each group.

2.4. Animal study

The rat implantation studies were performed following US National Institutes of Health guidelines for animal care, and were approved by the Institutional Animal Care and Use Committee of the University of Pittsburgh. The research was performed in compliance with the Animal Welfare Act Regulations and other Federal statutes

relating to animals and experiments involving animals and adhered to the principles set forth in the Guide for Care and Use of Laboratory Animals, National Research Council, 1996. Adult female Lewis rats were obtained from a local vendor (Harlan Sprague Dawley Inc., Indianapolis, IN, USA). For the abdominal wall reconstruction procedure, 10- to 12-week-old (200–250 g) rats were used.

The rats were anaesthetized with isoflurane (2.5% induction and 1.25–1.5% maintenance with 100% oxygen). The skin of the abdomen was shaved and sterilized with povidone-iodine solution. The surgical procedures performed were based on a previously reported approach (Hashizume *et al*., 2010). Approximately 2 cm inferior to the xiphoid process, a rectangular full-thickness defect (including abdominal wall fascia, muscle and peritoneum and excluding skin and subcutaneous tissue, 1.0 cm wide and 2.5 cm long) was dissected free from the abdominal viscera and removed. All abdominal wall defects were closed using identically sized patches generated for use in this study that were either the regionally distinct 'sandwich' type (with 20 min processing time for the upper and lower layers) or comprised dECM/PEUU without the upper and lower layers. Both patch types had the same thickness and both were oriented so that the axial direction of the collecting mandrel was aligned with the circumferential direction of the animal, and the circumferential direction of the mandrel was aligned with the animal's longitudinal axis upon patch implantation. The patches were sutured by a continuous 7-0 polypropylene suture to the remaining abdominal muscle and fascia without overlap between the muscle and patch and with direct contact to the subcutaneous tissue and the peritoneal viscera. The skin was then closed by double-layer buried suture. The rats were observed in the surgical suite until fully recovered from the anaesthesia. For postoperative treatment, buprenorphine (0.1 mg/kg) and cefuroxime (100 mg/kg) were administered subcutaneously and intramuscularly two times per day for 3 days after the procedure.

The implanted samples were surgically retrieved at 4 weeks or 8 weeks after implantation ($n = 7$ per group, per time-point). At retrieval, animals were euthanized by isoflurane (5%) inhalation and the abdominal wall was incised to expose the repaired site. Representative specimens were photographed *in situ* for later review and comparisons. The patches were explanted by cutting approximately 5 mm outside of the suture line. Subsequently, a 1×1 cm square shape was cut from each sample and used for measurements of the mechanical property of explants. Abdominal wall thickness was measured in these retrieved samples with a dial outside micrometer (L.S. Starrett Co., Athol, MA, USA); the remainder of the retrieved sample from all animals was processed for histological examination, immunostaining and collagen and elastin assays. To observe the change at a longer time-point (12 weeks), three rats were implanted with sandwich samples and three rats were implanted with control biohybrid samples for control purposes. These samples were explanted at 12 weeks and assessed only with macroscopic and histological evaluations.

2.5. Biaxial mechanical property measurements

Biaxial tensile mechanical measurements were performed for native tissues, for patches before implantation and for retrieved samples at each time-point (4 weeks and 8 weeks) utilizing a previously described method (Billiar and Sacks, 2000; Sacks, 2000). Briefly, samples were immersed in Ringer's solution (82 mM NaCl, 60 mM KCl, 2 mM $CaCl_2$, 10 mM Trizma-HCl, 10 mM Trizma-base, 11 mM dextrose) supplemented with verapamil (0.5 mM) and ethylene glycol tetraacetic acid (EGTA, 0.5 mM) for 1 h before testing to relax the muscle fibres completely. A 10×10 mm sample was removed from the explanted tissue for mechanical testing. Samples were floated in a room-temperature saline bath and tensile loading was applied equally to each axis up to a maximum Lagrangian membrane tension (T, force/unit length) of 200 N/m. This value was chosen based on previous results that indicate that this was the maximum tension that native rat abdominal wall tissue can reliably withstand without incurring damage. Four fiducial markers were affixed in a square configuration to the central region of each sample and were used to compute local strains as well as the deformation gradient tensor F. Circumferential and longitudinal axial stretches were determined from F11 and F22 respectively. Two 10-cycle equibiaxial tension protocols were performed. The first protocol was used to precondition the sample and data were recorded from the final cycle of the second protocol. Post processing was performed using a preconditioned free-float reference.

2.6. Histology, immunohistochemistry and collagen and elastin assays

For haematoxylin and eosin (H&E) and Masson's trichrome (MT) staining, the samples were fixed in 10% formalin solution for 24 h, embedded in paraffin, sectioned into 8-μm thick specimens and stained. For immunohistology, samples were fixed in 4% phosphate buffered paraformaldehyde for 2 h, immersed in 30% sucrose for 48 h then frozen and cryosectioned into 8-μm thick specimens. The primary antibodies used for immunohistochemical staining were: mouse anti-collagen I (Abcam, Cambridge, MA, USA) at 1:400 dilution; mouse anti-collagen III (Abcam) at 1:500 dilution; mouse anti-rat CD163 (Serotec, Oxford, UK) at 1:100 dilution; and rabbit anti-CCR7 (Abcam) at 1:250 dilution. The slides were counterstained with Hoechst 33342 (1 μg/ml; Invitrogen, Carlsbad, CA, USA). For each sample retrieved, 10 different microscopic fields were photographed for CD163- and CCR7-positive structures at $\times 100$ magnification and quantified using IMAGE J software, (National Institutes of Health, Bethesda, MD, USA).

The collagen and elastin content in explanted samples were measured using the Sircol collagen assay kit and the Fastin elastin assay kit (Accurate Chemical and Scientific Corp., Portsmouth, UK), respectively, following the manufacturer's instructions.

2.7. Two-photon microscopy

An Olympus FV 1000 multiphoton microscope (Center Valley, PA, USA) was used to detect the second harmonic generation signal from explanted constructs and native muscle. An excitation wavelength of 830 nm was used to elicit a collagen second harmonic generation signal based on previous reports (Cahalan *et al.*, 2002; Croix *et al.*, 2007). A depth of approximately 80–100 μm from the surface was scanned. Images were collected and processed into three-dimensional (3D) stacks using Imaris (Bitplane, Belfast, UK). The collagen network structure was assessed using a custom-made algorithm based on the intensity gradient texture analysis method (Chauduri *et al.*, 1993; Karlon *et al.*, 1998) which is able to capture the main angle of fibre orientation and the level of fibre alignment with respect to a detected preferred angle. The orientation index (OI) (Sacks and Chuong, 1992) was employed as a metric for fibre alignment, with OI = 0.5 reflecting a perfectly random (structural isotropy) fibre angle distribution and OI = 1 reflecting parallel fibres (a high level of structural anisotropy). A previously developed local thresholding method (D'Amore *et al.*, 2010) was adopted to enhance the collagen network signal against the background noise.

2.8. Statistical analyses

Statistical analyses were performed using IBM SPSS Statistics 19 (IBM, Armonk, NY, USA). Results are presented as mean ± standard error of the mean. One-way analysis of variance (ANOVA) followed by Tukey–Kramer multiple comparison testing was applied for comparison of multiple samples. To compare mechanical property measurements, one-way ANOVA was applied to compare the maximum stretch for each sample. Differences were considered to be statistically significant at $p < 0.05$.

3. Results

3.1. Effect of processing on scaffold mechanics

The sandwich samples had the appearance of white glistening sheets (Figure 1b), which was similar to that for control biohybrid scaffolds, although the former appeared to be slightly more opaque on the surface. Under scanning electron microscopy, the cross-section of the control (Figure 2a) seemed similar with the middle layer of gel/fibre hybrid in the sandwich scaffold (Figure 2b). The upper and lower electrospun layers of the sandwich scaffold (Figure 2c,d) were readily

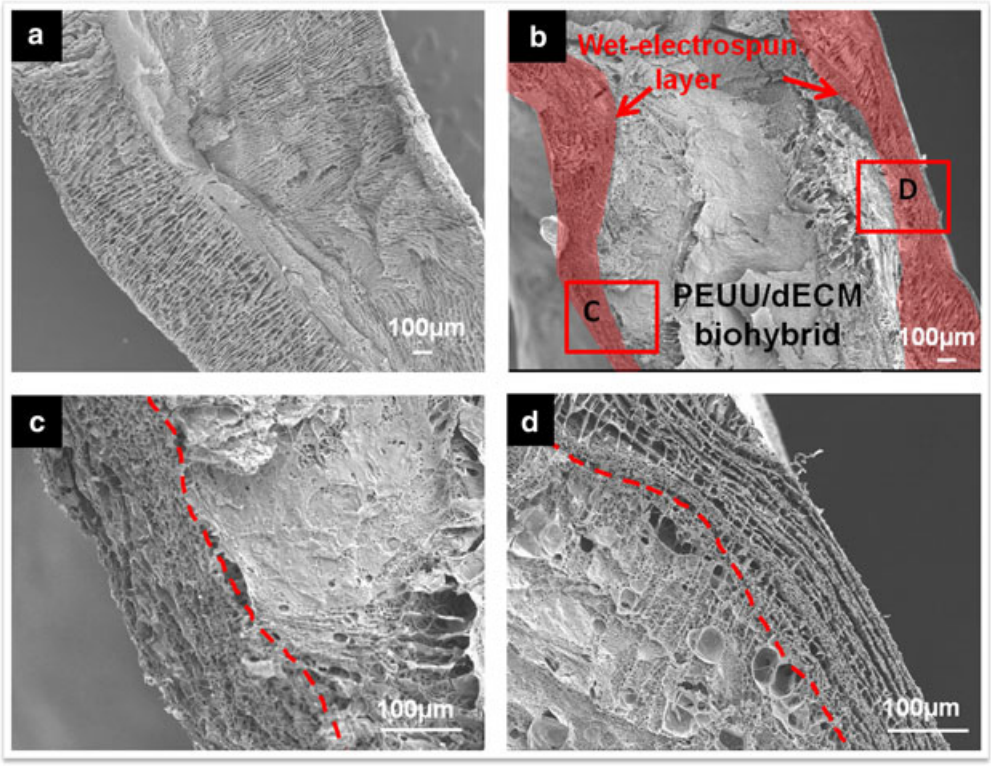

Figure 2. Electron micrographs of the control (a) and 'sandwich' scaffold (b,c,d) cross-sections. The upper and lower polymer-rich electrospun layers are readily identifiable with the middle extracellular matrix (ECM) gel/polymer layer showing markedly fewer and looser fibre-rich structures as the gel component was readily apparent. dECM, dermal extracellular matrix; PEUU, elastomeric poly(ester urethane)urea

identifiable with the middle ECM gel/polymer layer showing markedly fewer and looser fibre-rich structures as the gel component was readily apparent.

Alterations in the wet electrospinning time changed the mechanical properties of the scaffold and all materials exhibited anisotropic behaviour. By increasing the wet electrospinning time from 10 min to 30 min, peak tensile strengths of sandwich scaffolds increased significantly in both the longitudinal and circumferential directions (Figure 3a), and were significantly higher than for control

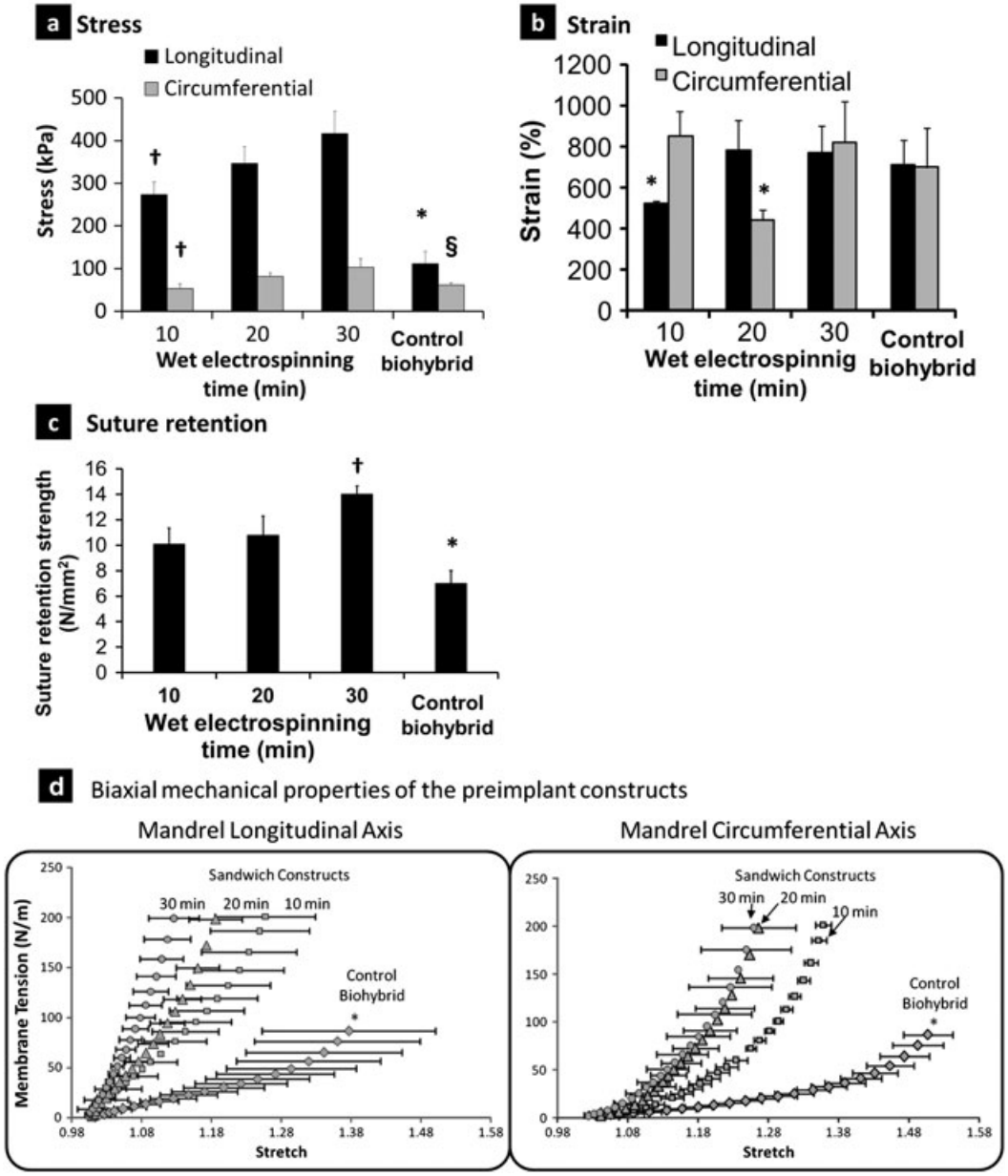

Figure 3. Mechanical properties of 'sandwich' scaffolds were altered by changing the wet electrospinning [phosphate-buffered saline (PBS) electrospraying] time. (a) Peak tensile stress for sandwich samples with different wet electrospinning times and control biohybrid material lacking the upper and lower polymer-rich regions. Statistical differences were found between samples with 10-, 20- or 30-min wet electrospinning time and control biohybrid samples, and between 10-min wet electrospinning time samples and 20- and 30-min wet electrospinning time samples in the longitudinal direction. In the circumferential direction, differences were found between 10-min wet electrospinning time samples and 20- and 30-min wet electrospinning time samples and between 30-min wet electrospinning time samples and control biohybrid samples. $^{\dagger}p < 0.05$ compared with 20- and 30-min samples in the corresponding direction. $^{*}p < 0.05$ compared with 10-, 20- and 30-min samples in the corresponding direction. $^{\S}p < 0.05$ compared with 30-min sample in the corresponding direction. (b) Peak tensile strain of sandwich and control biohybrid scaffolds. No obvious trends were apparent, although the 10-min and 20-min wet electrospinning time samples had lower peak tensile strains in the longitudinal and circumferential directions, respectively. $^{*}p < 0.05$ compared with other direction or samples. (c) In suture retention testing statistical differences were seen between 10- and 20-min wet electrospinning time samples and 30-min samples and between 10-, 20- and 30-min wet electrospinning time samples and control biohybrid samples. $^{\dagger}p < 0.05$ compared with 10- and 20-min samples. $^{*}p < 0.05$ compared with 10-, 20- and 30-min samples. (d) Pre-implant biaxial tensile testing showed statistical differences between all of the sandwich samples and control biohybrid samples in both directions. $^{*}p < 0.05$ compared with 10-, 20- and 30-min samples

DOI: 10.1002/term

biohybrid scaffolds in the corresponding directions. Peak strains of all samples were greater than 400% in both directions (Figure 3b). Suture retention strength was also increased with the regionally distinct scaffold processing (Figure 3c). Increasing the wet electrospinning time had minimal effect on overall scaffold thickness (on the order of tens of microns), which did not contribute substantially to the overall thickness of the scaffolds (2–2.5 mm). Under equibiaxial stretching the anisotropic behaviour observed in the unidirectional testing was much less pronounced for all scaffolds (Figure 3d).

3.2. Macroscopic observations after implantation period

No notable tissue adhesion to intraperitoneal organs was observed, except for slight adhesions to the omentum or mesentery. No clinical infections were observed at any point after patch implantation (Figure 4a). The thickness of the sandwich samples decreased significantly from pre-implant to the 8-week time-point, but not significantly from pre-implant to 4 weeks, or from 4 weeks to 8 weeks. The thickness of the control biohybrid patches at 4 weeks had thinned from pre-implant values to similar to that of native tissue, while at 8 weeks the explants had further thinned to approximately half of the native wall thickness (Figure 4b). The control explants were significantly thinner than sandwich samples at the 4-, 8- and 12-week time-points. The control group experienced abdominal herniation in three out of seven animals (42.9%) at 8 weeks and two out of three at 12 weeks, all of which occurred at the middle of the patch not the junctions. No herniation was observed in the sandwich group.

3.3. Histological assessment

Histological assessment showed that both scaffold types had extensive cellular infiltration at both time-points (Figure 5a). The thinning of the control scaffold was readily observable in cross-sectional histological mosaics at 8 weeks and 12 weeks. At higher magnification, the extensive cellular infiltration was seen again in both scaffold types at 4-, 8- and 12-week explants. Vascular ingrowth was observed in both scaffold types at both time-points; Masson's trichrome staining also consistently showed collagen deposition within the construct for both scaffold types at 4-, 8- and 12-week explants (Figure 5b).

3.4. Explanted construct mechanical properties

Biaxial mechanical testing of explanted constructs demonstrated a pronounced stiffening ($p < 0.05$) of all scaffolds compared with the pre-implant mechanical response (Figure 6). At 4 weeks, both sandwich scaffolds and control biohybrid scaffolds possessed a moderate degree of mechanical anisotropy in a similar manner to that of native tissue, however, both scaffold types were, in general, less compliant. Following 8 weeks *in vivo*, the sandwich scaffolds displayed higher levels of mechanical anisotropy than control biohybrid scaffolds through a significantly more compliant longitudinal axis ($p < 0.05$).

3.5. Collagen and elastin assays

Collagen assays showed a marked increase in total collagen content for both patch types from the time of implant to 4 weeks and 8 weeks ($p < 0.01$, Figure 7a). The amount

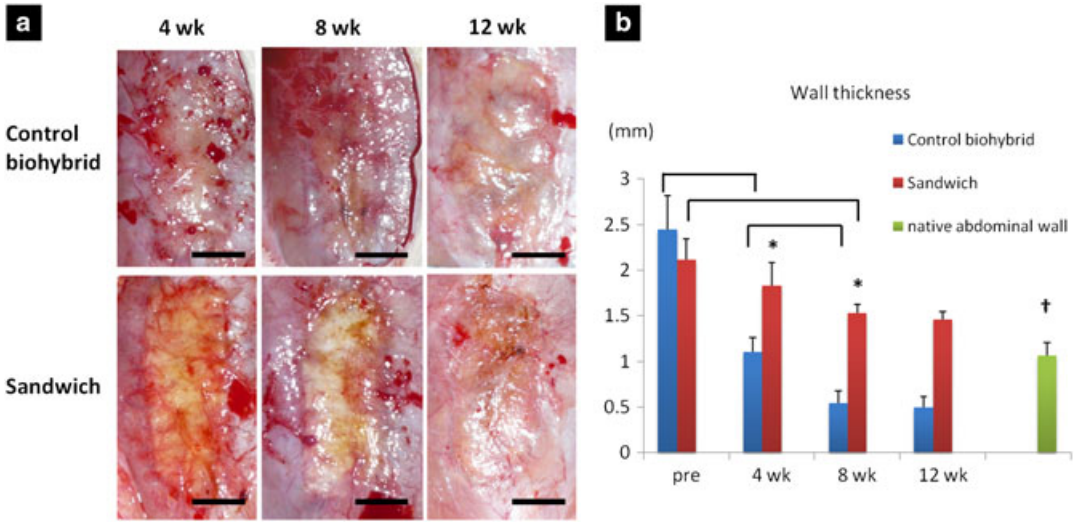

Figure 4. (a) Gross observations of the scaffolds retrieved 4, 8 and 12 weeks after implantation. Abdominal herniation was seen in three of seven samples (43%) in the control biohybrid group at 8 weeks, and two out of three at 12 weeks, while no herniation was seen in the 'sandwich' group (scale bar = 1 cm). (b) Wall thickness of pre-implant and 4-, 8- and 12-week explanted samples. The thickness of the sandwich samples decreased significantly from pre-implant to the 8-week time point, but not significantly from pre-implant to 4 weeks and from 4 weeks to 8 weeks. The thickness of the control biohybrid patches at 4 weeks had thinned from pre-implant values to be similar to that of native tissue, while at 8 weeks the explants had further thinned to approximately half of the native wall thickness. *$p < 0.05$ compared with control biohybrid samples at the same time point. †$p < 0.05$ compared with all the experimental samples except the 4-week control biohybrid sample

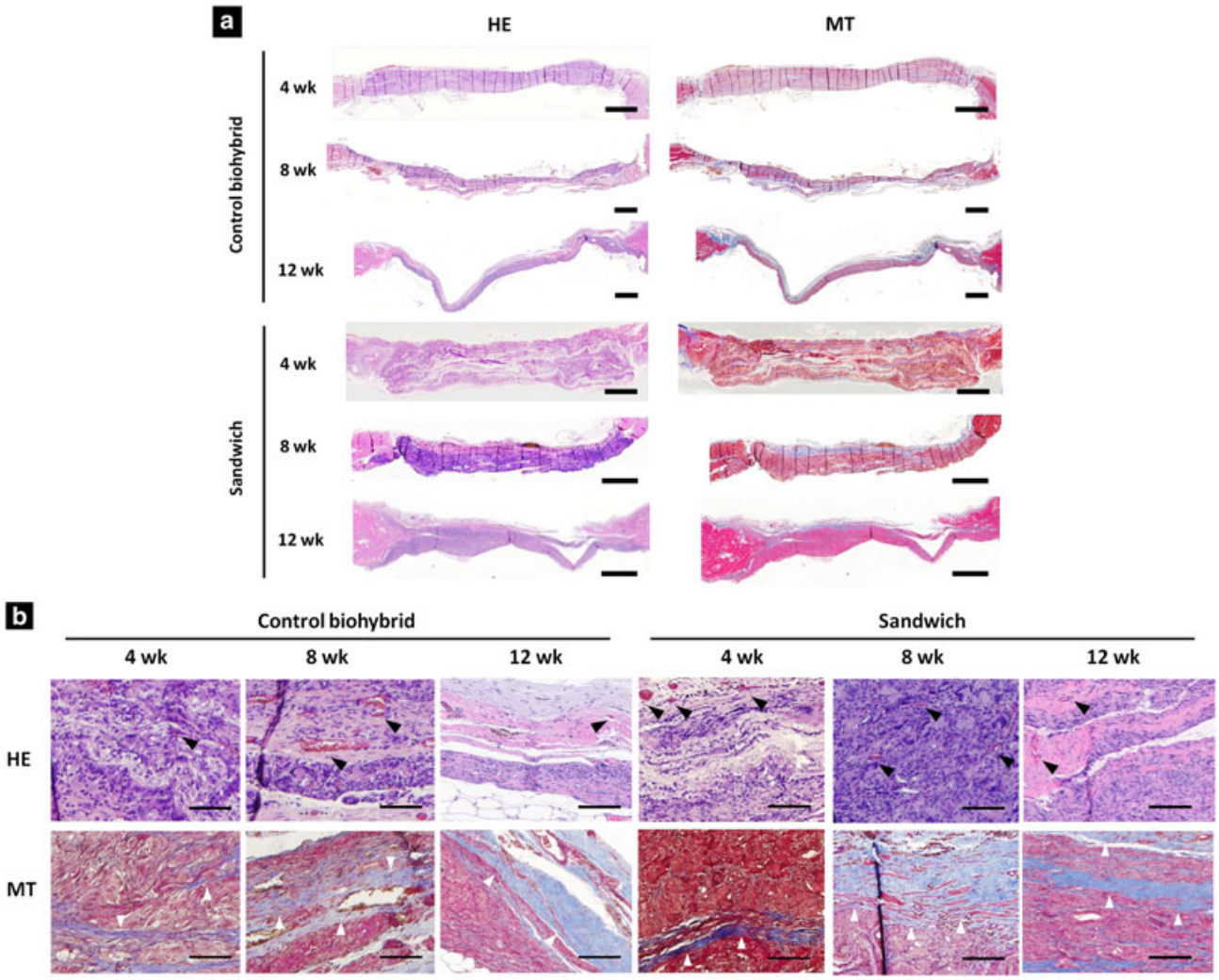

Figure 5. (a) Representative cross-sections of control biohybrid and 'sandwich' samples stained with haematoxylin and eosin, and Masson's trichrome at 4-, 8- and 12-weeks time-points (scale bar = 1 mm). Both scaffold types had extensive cellular infiltration at both time-points. The thinning of the control scaffold was readily observable in the cross-sectional image at 8 weeks while the sandwich sample largely maintained its thickness. (b) Vascular ingrowth was also observed in both scaffold types at both time-points and Masson's trichrome staining consistently showed collagen deposition within the construct for both scaffold types at 4, 8 and 12 weeks (scale bar = 200 μm). Vessels in the samples are indicated with black arrowheads and connective fibres (collagen) are indicated with white arrowheads

of collagen was greater in the sandwich group compared with the control biohybrid group for both time-points ($p < 0.05$), although neither of the explanted patches achieved collagen content equivalent to that of the native abdominal muscle. There were no significant trends for elastin content in the samples from 4 weeks to 8 weeks (Figure 7b), although the elastin content increased significantly from the time of implantation in both types.

3.6. Immunohistochemical assessment and two-photon microscopy

Immunohistochemical staining of the explants for collagen types I and III showed that collagen I was predominantly evident at the construct periphery, while collagen III was found throughout the implant (Figure 8). The collagen I-rich area corresponds to the surface layer scanned by multiphoton microscopy for the assessment of collagen network structure.

Two-photon micrograph images of the native abdominal muscle, 4-week sandwich and 8-week sandwich samples were assessed to investigate the structural arrangement of collagen fibres (Figure 9a,c). Quantitative analysis of the collagen fibre angle distribution at each time-point (Figure 9 e–g) showed levels of structural anisotropy consistent between the three groups (OI = 0.58 for native abdominal muscle, 0.61 for 4-week sandwich and 0.59 for 8-week sandwich). The orientation index levels detected indicated anisotropy ($0.55 \leq OI \leq 0.65$), which is comparable to previous studies (Agoram and Barocas, 2001; D'Amore *et al.*, 2010) and typically associated with a physiologically relevant level of mechanical anisotropy.

Assessment of scaffold site remodelling with immunostaining for macrophage phenotype showed that the ratio of CD163-positive cells (M2 macrophages) versus CCR7-

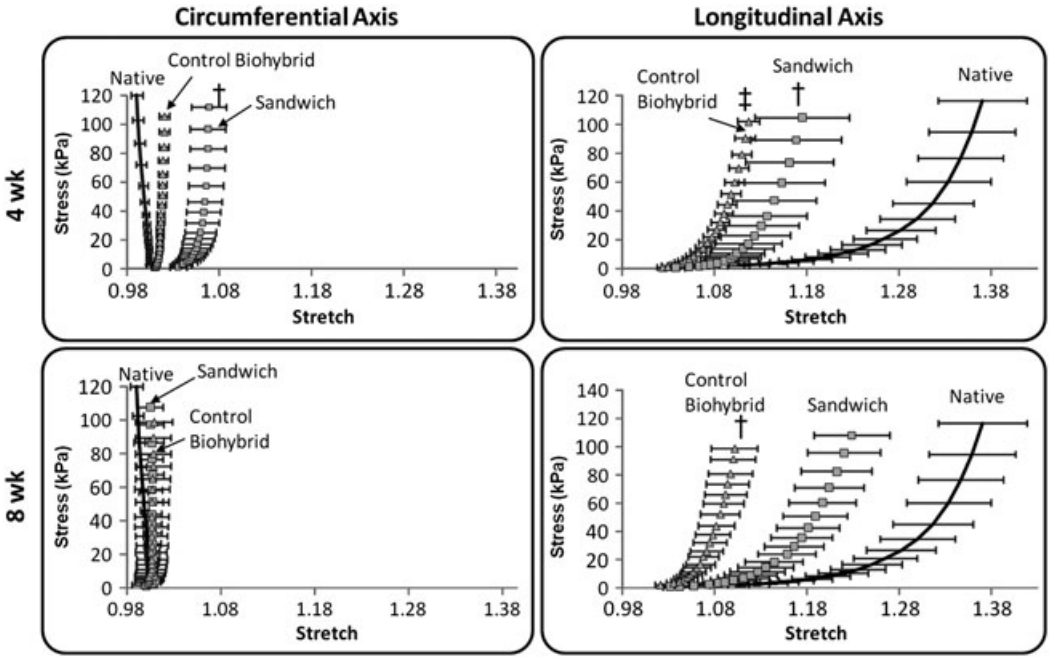

Figure 6. Biaxial mechanical testing of explanted constructs demonstrated a pronounced stiffening of all scaffolds compared with the pre-implant mechanical response. At 4 weeks, both sandwich scaffolds and control biohybrid scaffolds possessed a moderate degree of mechanical anisotropy in a manner similar to native tissue; however, both scaffold types were, in general, less compliant. Following 8 weeks *in vivo*, the sandwich scaffolds displayed higher levels of mechanical anisotropy than control biohybrid scaffolds through a significantly more compliant longitudinal axis. $^{\dagger}p < 0.05$ compared with native tissue; $^{\ddagger}p < 0.05$ compared with sandwich sample and $p < 0.01$ compared with native tissue

positive cells (M1 macrophages) increased in the sandwich group from 4 weeks to 8 weeks, and at 8 weeks was greater than that observed in biohybrid control constructs (Figure 10).

4. Discussion

The extracellular matrix and its derivative ECM gel have promising characteristics for tissue engineering. In many studies, growth factors, such as basic fibroblast growth factor (bFGF), vascular endothelial growth factor (VEGF) and transforming growth factor-beta (TGF-β), released from ECM, as well as ECM degradation products have been shown to promote tissue regeneration or to act as chemoattractants for progenitor cells from various mature organs and differentiated cells (Li *et al*., 2004; Hodde *et al*., 2005; Reing *et al*., 2009). This material class also works as a biological scaffold for migrating cells as it contains structural fibres such as collagen, elastin and fibronectin. Moreover, non-crosslinked ECM scaffolds have been shown to modulate the inflammatory response from the body, eliciting a more prominent M2 macrophage phenotype, which has been associated with constructive ECM and functional remodelling of the tissue, including organized connective tissue and vasculature (Badylak *et al*., 2008; Brown *et al*., 2009).

In clinical ventral hernia repair, allogenic or xenogenic extracellular matrix products have been increasingly used as replacement (interpositional), overlay or underlay materials (Butler *et al*., 2005; Gupta *et al*., 2006; Espinosa-de-los-Monteros *et al*., 2007; Nemeth and Butler, 2009). Some reports showed successful outcomes when large, complex abdominal wall defects were reconstructed with acellular dermal matrix, even when placed directly over viscera and when the operative field was irradiated or contaminated (Butler *et al*., 2005; Nemeth and Butler, 2009). Although the use of ECM in the abdominal interpositional setting still remains controversial (Zhong *et al*., 2011), it is widely accepted that it will improve integration with surrounding tissues and vasculature.

The recurrence of an abdominal hernia is known to be related to an improper ratio of collagen isoforms, resulting in a weakened body wall (Franz, 2006). Many reports have shown such a collagen isoform change in the muscle, subcutaneous tissue or skin in patients with inguinal hernia or uterine prolapsed (Klinge *et al*., 1999a,1999b, 2000; Rosch *et al*., 2002; Taniguchi *et al*., 2006) showing that the type I collagen, which usually is the most abundant subtype and represents a load-bearing, cross-linked isoform, will decrease and type III collagen, which is less cross-linked and provides less tensile strength, will increase. Type III collagen is characteristically abundant in the early stage of wound healing and is subsequently replaced by type I collagen. The data did not show obvious differences in the relative expression amounts or patterns of type I and type III collagen when comparing scaffold types. Longer implant times might be needed to better investigate this aspect of the scaffold remodelling response. In addition, because the animal

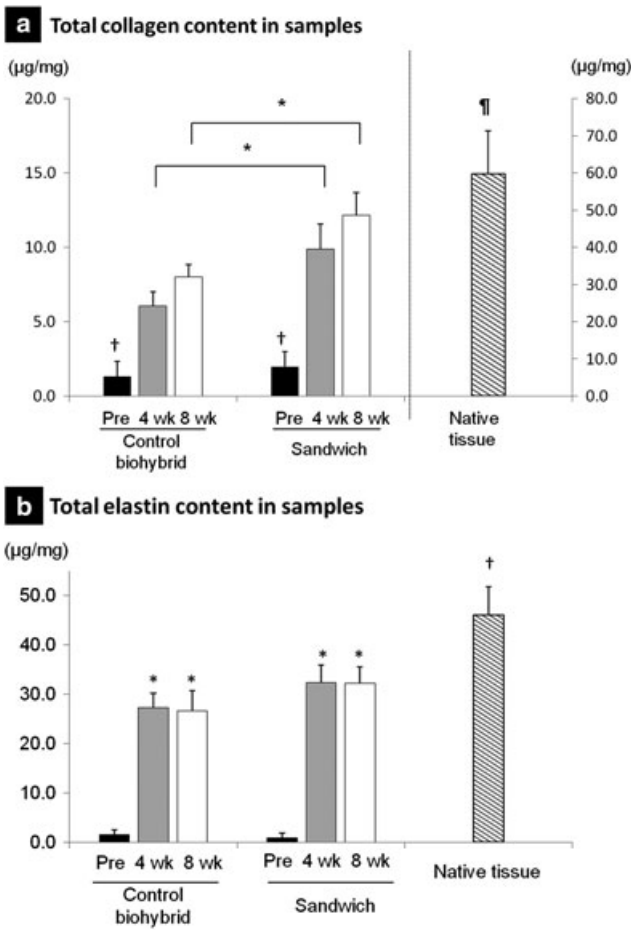

Figure 7. (a) Collagen content in samples. The collagen content in both scaffold types markedly increased after implantation. The left axis scale applies to the experimental groups and the right axis scale applies to the native tissue. *$p < 0.05$ between control biohybrid and sandwich scaffolds at same time-point. †$p < 0.01$ compared with 4- and 8-week samples. ¶$p < 0.01$ compared with preimplant samples; and $p < 0.05$ compared with 4- and 8-week samples in experimental groups. (b) Elastin content in samples. The elastin content of the sample markedly increased after implantation. *$p < 0.01$ compared with preimplant; †$p < 0.01$ compared with preimplant; and $p < 0.05$ compared with 4- and 8-weeks samples in experimental groups

model employed lacks an inherent tendency to develop weakened tissue structures, it may provide limited insight into how patients with such conditions might ultimately remodel such scaffolds. Several animal models that create intra-abdominal hypertension have been reported, including the injection of saline (Du *et al*., 2012), gas (He *et al*., 2012) or oil (Hamidian Jahromi *et al*., 2012) into the intraperitoneal cavity. Employing such animal models to assess the effect of hypertension on construct healing under elevated pressures would provide further insight into the healing response and applicability of the method in challenging clinical settings.

While ECM has attractive bioactivity and, in many instances, may provide mechanical outcomes that are desirable, there would be interest in broadening and tuning the mechanical behaviour of ECM-based materials by the formation of biocomposites. Electrospun PEUU has mechanical properties that are consistent with some soft tissues, as has been described previously (Stankus *et al*., 2008; Hong *et al*., 2009, 2011, 2012; Hashizume *et al*., 2010). In earlier reports these two materials were either directly combined and the mixture electrospun (Hong *et al*., 2012), or were integrated using independent deposition pathways (electrospinning with concurrent electrospraying) (Hong *et al*., 2011). Although the latter technique had more attractive initial healing properties, longer-term implants with this material in the current report showed that the incidence of mechanical failure increased markedly at 8 weeks. To overcome this phenomenon, two general strategies might come to mind. First, the polymer mass fraction might be increased throughout the composite to create a material that increasingly approaches the mechanical properties of the polymeric component. The second approach would be to similarly increase the polymer fibre content, but to do so in a spatially distinct manner, adding supportive, polymer-rich layers and maintaining the higher ECM content of the inner layer. Pursuing the latter approach, fibre-rich layers were generated at the beginning and at the end of the deposition process. Instead of simply electrospinning PEUU for these layers, however, PBS was electrosprayed concurrent with PEUU fibre deposition. This wet electrospinning technique was done as a previous report where culture medium was electrosprayed concurrently with fibre deposition resulted in a scaffold that was markedly more amenable to tissue infiltration, putatively because of a looser fibre structure being deposited in the wet conditions (Hashizume *et al*., 2010). A simple single layer of this wet electrospun PEUU would be an alternative control for current study. When compared with this previously reported scaffold, although the histological appearance of the constructs at 4 weeks and 8 weeks looked similar, the mechanical properties at the time of explant showed more anisotropic behaviour and better mimicry of the native abdominal wall in the current report, implying that, at least from a mechanical perspective, a more desirable remodelling outcome.

Consistent with previous reports (Hong *et al*., 2008, 2009; Hashizume *et al*., 2010), the mechanical properties of the scaffold changed over the implantation period. The design used in the *in vivo* experiment used 20 min of wet electrospinning (to form the polymer layers). The mechanical properties of the construct were almost isotropic before implant (Figure 3d). However, at explant the biaxial tensile mechanical properties in the sandwich scaffold showed anisotropic behaviour that mimicked the passive native abdominal wall well, whereas for the control biohybrid construct sample this anisotropy was not as pronounced (Figure 6). An implication of this result is that the *in vivo* milieu, including the mechanical loading which would occur there, created a scaffold remodelling environment with cell infiltration, extracellular matrix elaboration and degradation of the implanted scaffold components that resulted in remodelling towards passive mechanical properties similar to the native tissue. This was concurrent with increased collagen content and M2 macrophage presence in the sandwich group.

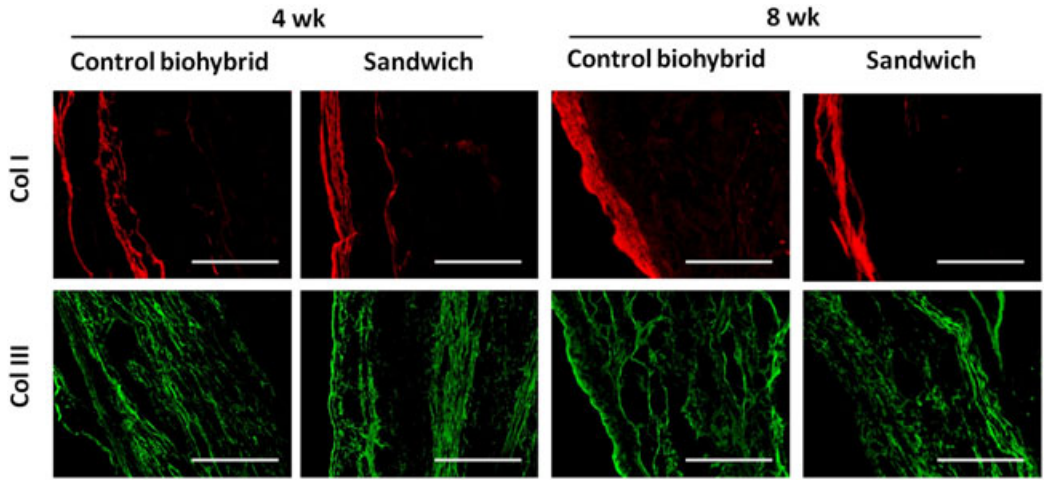

Figure 8. Immunostaining for type I (Col1, red) and type III collagen (Col3, green) for control biohybrid and sandwich samples at 4 weeks and 8 weeks. Collagen I was predominantly evident at the construct periphery, while collagen III was found throughout the implant (scale bar = 200 μm).

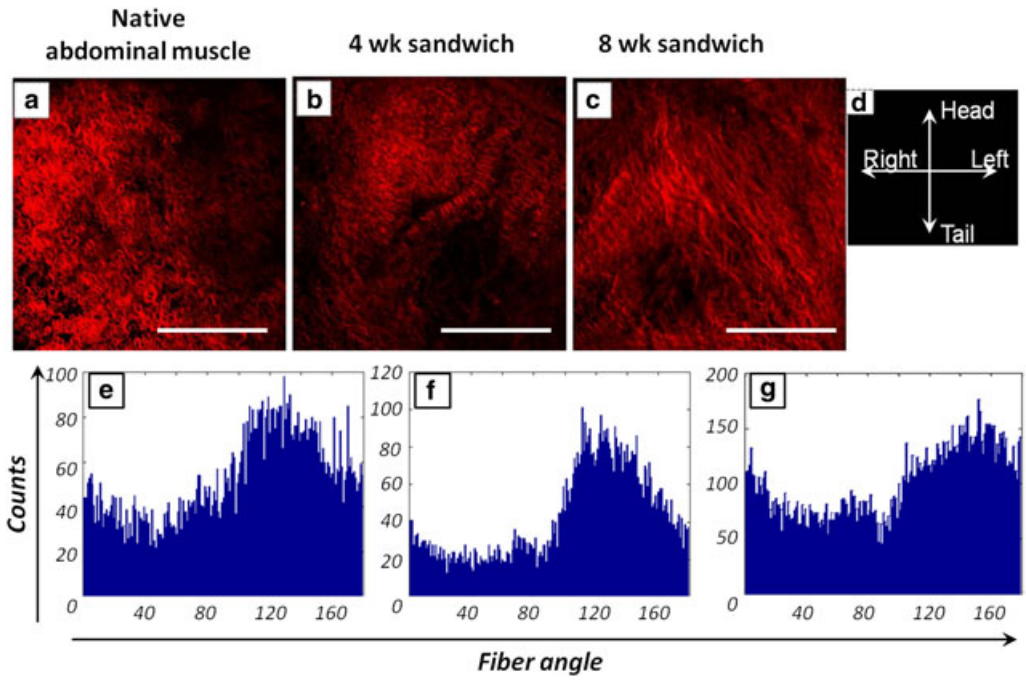

Figure 9. (a–c) Two-photon micrographs showing collagen fibres in the native abdominal muscle (a), 4-week (b) and 8 week sandwich (c) samples (scale bar = 200 μm). (d) Animal orientation in the previous images. (e–g) Analysis of the collagen fibre direction in each group. A similar pattern of collagen structural anisotropy was observed between native abdominal muscle (e), and the 4-week (f) and 8-weeks (g) sandwich explanted constructs

The lower concentrations of collagen deposited for the control biohybrid versus sandwich scaffolds may be a contributory reason for the former group failing to maintain its wall thickness and experiencing a higher incidence of failure at later time-points. For both groups, type I collagen was dominant in the outer layer and type III collagen was dominant in inner layer in all the samples, suggesting that maturation of the tissue construct occurs from the periphery. The structural similarity of the collagen deposited in the sandwich sample to that in native tissue was further evaluated by two-photon micrographs and quantification of extracellular matrix fibre orientation. Four- and eight-week explants showed a similar structural anisotropy to native rectus abdominal muscle tissue. The failure of the biohybrid scaffolds may be related to increased wall stresses experienced because of the lack of supporting structures in the top and bottom layers. This increased stress may have negatively influenced the ability of the ingrowing tissue to synthesize adequate or appropriate ECM components, including collagen (Klinge *et al.*, 2006).

The structure of the scaffold employed also appeared to have an effect on the macrophage phenotype at longer implant times. Macrophages have been shown to play a key role in the regeneration of injured muscle tissue. Proinflammatory (M1) macrophages infiltrate into the

DOI: 10.1002/term

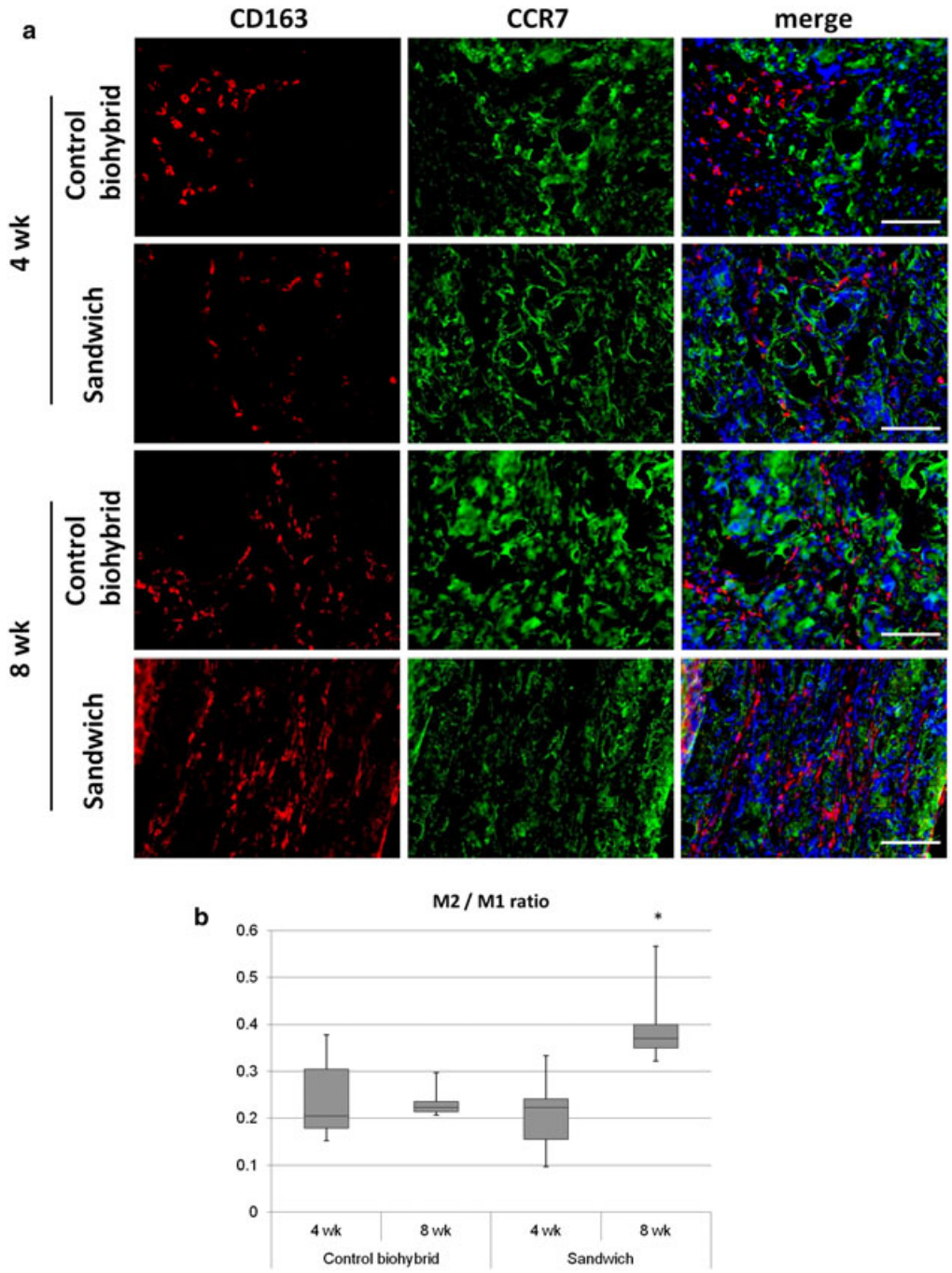

Figure 10. (a) Immunostaining for CCR7 (green, M1 macrophage) and CD163 (red, M2 macrophage). Nuclei are stained with Hoechst (blue) (scale bar = 200 μm). (b) M2 to M1 ratio in the cross-sectional sample. The ratio increased in the sandwich group from 4 weeks to 8 weeks, and at 8 weeks was greater than that observed in the biohybrid control constructs. *$p < 0.05$ for the 8-week sandwich group vs. the 4-week sandwich group and both biohybrid time-points

injured tissue and remove damaged cells and tissue. The increased presence of anti-inflammatory, 'remodelling' (M2) macrophages that are induced by anti-inflammatory cytokines such as interleukin (IL)-4, IL-10 and TGF-β are believed to be an important component of constructive remodelling. The M2 macrophages attenuate M1 macrophage proliferation by releasing anti-inflammatory cytokines (IL-4, 10 and TGF-β) and promoting myogenic differentiation, which is seen in the elevation of myogenic marker expression such as myogenin and MyoD, and fusion of myofibres (Tidball and Wehling-Henricks, 2007; Badylak *et al*., 2008; Ruffell *et al*., 2009; Ten Broek *et al*., 2010). In the present study, the M2 macrophage phenotype was relatively elevated with respect to the M1 phenotype at 8 weeks for the sandwich scaffolds vs. the biohybrid controls. This finding is interesting, as the original components of the scaffolds were the same but the regional increase in the polymer component resulted in a modified response. A possibility is that the mechanical load, which would vary between the scaffolds during the implant period, affects the nature of the inflammatory and remodelling response. Further investigation of this

phenomenon might include more extensive analysis of M2 subgroups and the evaluation of functional markers to better relate the temporal course of the macrophage infiltrate with remodelling outcomes (Brown *et al*., 2012).

In the animal model employed in the study, it is considered that the tissue ingrowth may occur from all sides except the intraperitoneum when there are no adhesions of intraperitoneal organs and from all sides when there are some adhesions of intraperitoneal organs such as omentum and mesentery. However, in the abdominal wall, the peripheral muscle tissue is likely of primary importance in the remodelling response, both because of the design of the scaffold and because this is the tissue that would be the putative source of musculogenic healing for small abdominal wall trauma. The sandwich scaffold would have easier access for cell migration from the sides vs. the top and bottom layers, as can be appreciated in examining the cross-section images in Figure 2. The middle layer has a lower density of fibres and is open only on the periphery of the scaffold.

Several limitations and opportunities following from the current report should be mentioned. No substantial functional skeletal muscle formation was observed, except for a limited amount of regional muscle growth from the surrounding muscle stump during the period of observation. It would be worthwhile to examine longer periods post-implantation to evaluate skeletal muscle regeneration, and to examine the effect of a muscle onlay or underlay on this remodelling response. Alternative ECM sources, such as skeletal muscle (Wolf *et al*., 2012) would possibly enhance the development toward functional muscle tissue. The rodent model is limited to relatively short-term investigations by its nature, but, in the clinical setting, the effect on the remodelling process would need to be determined over years. Larger animal models with long-term observation periods would be important to evaluate the long-term physiological response. The model used in the current study was a full-thickness abdominal wall reconstruction, but the approach to discriminate between the mechanically supportive region and bioactive region within one scaffold might ultimately be applicable to other target diseases and organs, such as pelvic floor prolapse, breast reconstruction and urinary incontinence.

It is still unclear as to how long the load-bearing components of the scaffold need to remain in place before this load can be adequately taken on by host tissue. The ideal time for material degradation would depend upon the body forces experienced and the type and amount of surrounding tissue generated in the healing response. Too rapid degradation appears to lead to thinning and failure, therefore non-degrading or slowly degrading materials may be better, although achieving host tissue capable of full load-bearing may be inhibited by synthetic components that effectively act to shield the tissue from stress. To examine this effect one might employ alternative chemistries for biodegradable polyurethanes that provide similar mechanical properties, but exhibit more rapid, or slower degradation (Guan *et al*., 2005; Hong *et al*., 2010). Further study in this area is clearly needed.

5. Conclusions

Co-electrospinning–electrospraying was employed to create a 'sandwich' scaffold that combined porcine dermal ECM gel with biodegradable elastic PEUU, where a dermal ECM gel-enriched layer was sandwiched by two PEUU-rich layers. The PEUU-rich layers provided improved mechanical strength while the dECM-rich layer provided a potential source for bioactive components. *In vivo* evaluation comparing the sandwich scaffold with a control biohybrid scaffold without the upper and lower regions showed a marked increase in collagen content while preserving good cellular infiltration in the former, and thinning with multiple mechanical failures in the latter after 8 weeks. At explant the biaxial tensile mechanical behaviour of the sandwich scaffold mimicked the structural and mechanical anisotropy of the native abdominal wall. By employing a processing approach that creates a sheet-form scaffold with regionally distinct zones, it was possible to improve biological outcomes in body wall repair and provide the means for further tuning of scaffold mechanical parameters when targeting other applications.

Conflict of interest

The authors have declared that there is no conflict of interest.

Acknowledgements

This work was supported in part by the Armed Forces Institute for Regenerative Medicine (AFIRM, #W81XWH-08-2-0032) and C.R. Bard, Inc. We also thank Prof. Michael S. Sacks for use of the biaxial mechanical testing device, Deanna Rhoads and Hongbin Jiang for histological sectioning and Greg Gibson for multiphoton imaging.

References

Agoram B, Barocas VH. 2001; Coupled macroscopic and microscopic scale modeling of fibrillar tissues and tissue equivalents. *J Biomech Eng* **123**: 362–369.

Badylak SF, Valentin JE, Ravindra AK *et al*. 2008; Macrophage phenotype as a determinant of biologic scaffold remodeling. *Tissue Eng Part A* **14**: 1835–1842.

Badylak SF, Weiss DJ, Caplan A *et al*. 2012; Engineered whole organs and complex tissues. *Lancet* **379**: 943–952.

Billiar KL, Sacks MS. 2000; Biaxial mechanical properties of the native and glutaraldehyde-treated aortic valve cusp: Part II – a structural constitutive model. *J Biomech Eng* **122**: 327–335.

Brown BN, Valentin JE, Stewart-Akers AM *et al*. 2009; Macrophage phenotype and remodeling outcomes in response to biologic scaffolds with and without a cellular component. *Biomaterials* **30**: 1482–1491.

Brown BN, Londono R, Tottey S *et al*. 2012; Macrophage phenotype as a predictor of constructive remodeling following the implantation of biologically derived surgical mesh materials. *Acta Biomater* **8**: 978–987.

Butler CE, Langstein HN, Kronowitz SJ. 2005; Pelvic, abdominal, and chest wall reconstruction with AlloDerm in patients at increased risk for mesh-related complications. *Plast Reconstr Surg* **116**: 1263–1275.

Cahalan MD, Parker I, Wei SH *et al*. 2002; Two-photon tissue imaging: seeing the immune system in a fresh light. *Nat Rev Immunol* **2**: 872–880.

Cassar K, Munro A. 2002; Surgical treatment of incisional hernia. *Br J Surg* **89**: 534–545.

Chauduri BB, Kundo PK, Nirupam S. 1993; Detection and gradation of oriented texture. *Pattern Recogn Lett* **14**: 147–153.

Croix CS, Zipfel WR, Watkins SC. 2007; Potential solutions for confocal imaging of living animals. *Biotechniques* **43**: 14–19.

D'Amore A, Stella JA, Wagner WR *et al*. 2010; Characterization of the complete fiber network topology of planar fibrous tissues and scaffolds. *Biomaterials* **31**: 5345–5354.

den Hartog D, Dur AH, Tuinebreijer WE *et al*. 2008; Open surgical procedures for incisional hernias. *Cochrane Database Syst Rev* **16**: CD006438.

Du WH, Xiang W, Liu DC *et al*. 2012; Usefulness of speckle tracking imaging to assess myocardial contractility in intra-abdominal hypertension: study in a mini-pig model. *Cell Biochem Biophys* **64**: 123–129

Dumanian GA, Denham W. 2003; Comparison of repair techniques for major incisional hernias. *Am J Surg* **185**: 61–65.

Espinosa-de-los-Monteros A, de la Torre JI, Marrero I *et al*. 2007; Utilization of human cadaveric acellular dermis for abdominal hernia reconstruction. *Ann Plast Surg* **58**: 264–267.

Franz MG. 2006; The biology of hernias and the abdominal wall. *Hernia* **10**: 462–471.

Guan J, Sacks MS, Beckman EJ *et al*. 2002; Synthesis, characterization, and cytocompatibility of elastomeric, biodegradable poly (ester-urethane)ureas based on poly (caprolactone) and putrescine. *J Biomed Mater Res* **61**: 493–503.

Guan J, Fujimoto KL, Sacks MS *et al*. 2005; Preparation and characterization of highly porous, biodegradable polyurethane scaffolds for soft tissue applications. *Biomaterials* **26**: 3961–71.

Gupta A, Zahriya K, Mullens PL *et al*. 2006; Ventral herniorrhaphy: experience with two different biosynthetic mesh materials, Surgisis and Alloderm. *Hernia* **10**: 419–425.

Hamidian Jahromi A, Freeland K, Youssef AM. 2012; Intra-abdominal hypertension causes disruption of the blood–brain barrier in mice, which is increased with added severe head trauma. *J Trauma Acute Care Surg* **73**: 1175–1179

Hashizume R, Fujimoto KL, Hong Y *et al*. 2010; Morphological and mechanical characteristics of the reconstructed rat abdominal wall following use of a wet electrospun biodegradable polyurethane elastomer scaffold. *Biomaterials* **31**: 3253–3265.

He Q, Cai L, Zhang S *et al*. 2012; Oxygen inhalation improves survival time of mice with acute intra-abdominal hypertension and protects liver cells. *Transplant Proc* **44**: 1201–1205

Hodde JP, Record RD, Liang HA *et al*. 2001; Vascular endothelial growth factor in porcine-derived extracellular matrix, *Endothelium* **8**: 11–24.

Hodde JP, Ernst DM, Hiles MC. 2005; An investigation of the long-term bioactivity of endogenous growth factor in OASIS Wound Matrix. *J Wound Care* **14**: 23–25.

Hong Y, Fujimoto K, Hashizume R *et al*. 2008; Generating elastic, biodegradable polyurethane/poly(lactide-co-glycolide) fibrous sheets with controlled antibiotic release via two-stream electrospinning. *Biomacromolecules* **9**: 1200–1207.

Hong Y, Ye SH, Nieponice A *et al*. 2009; A small diameter, fibrous vascular conduit generated from a poly(ester urethane) urea and phospholipid polymer blend. *Biomaterials* **30**: 2457–2467.

Hong Y, Guan J, Fujimoto KL *et al*. 2010; Tailoring the degradation kinetics of poly (ester carbonate urethane)urea thermoplastic elastomers for tissue engineering scaffolds. *Biomaterials* **31**: 4249–4358.

Hong Y, Huber A, Takanari K *et al*. 2011; Mechanical properties and *in vivo* behavior of a biodegradable synthetic polymer microfiber–extracellular matrix hydrogel biohybrid scaffold. *Biomaterials* **32**: 3387–3394.

Hong Y, Takanari K, Amoroso NJ *et al*. 2012; An elastomeric patch electrospun from a blended solution of dermal extracellular matrix and biodegradable polyurethane for rat abdominal wall repair. *Tissue Eng Part C Methods* **18**: 122–132.

Karlon WJ, Covell JW, McCulloch AD *et al*. 1998; Automated measurement of myofiber disarray in transgenic mice with ventricular expression of ras. *Anat Rec* **252**: 612–625.

Klinge U, Zheng H, Si Z *et al*. 1999a; Expression of the extracellular matrix proteins collagen I, collagen III and fibronectin and matrix metalloproteinase-1 and -13 in the skin of patients with inguinal hernia. *Eur Surg Res* **31**: 480–490.

Klinge U, Zheng H, Si ZY *et al*. 1999b; Synthesis of type I and III collagen, expression of fibronectin and matrix metalloproteinases-1 and -13 in hernial sac of patients with inguinal hernia. *Int J Surg Invest* **1**: 219–227.

Klinge U, Si ZY, Zheng H *et al*. 2000; Abnormal collagen I to III distribution in the skin of patients with incisional hernia. *Eur Surg Res* **32**: 43–48.

Klinge U, Binnebösel M, Rosch R *et al*. 2006; Hernia recurrence as a problem of biology and collagen. *J Minim Access Surg* **2**: 151–4.

Li F, Li W, Johnson S, Ingram D, Yoder M, Badylak S. 2004; Low-molecular-weight peptides derived from extracellular matrix as chemoattractants for primary endothelial cells. *Endothelium* **11**: 199–206.

Mudge M, Hughes LE. 1985; Incisional hernia: a 10 year prospective study of incidence and attitudes. *Br J Surg* **72**: 70–71.

Nemeth NL, Butler CE. 2009; Complex torso reconstruction with human acellular dermal matrix: long-term clinical follow-up. *Plast Reconstr Surg* **123**: 192–196.

Reing JE, Zhang L, Myers-Irvin J *et al*. 2009; Degradation products of extracellular matrix affect cell migration and proliferation. *Tissue Eng Part A* **15**: 605–614.

Reing JE, Brown BN, Daly KA *et al*. 2010; The effects of processing methods upon mechanical and biologic properties of porcine dermal extracellular matrix scaffolds. *Biomaterials* **31**: 8626–8633.

Rosch R, Klinge U, Si Z *et al*. 2002; A role for the collagen I/III and MMP-1/-13 genes in primary inguinal hernia? *BMC Med Genet* **3**: 2.

Ruffell D, Mourkioti F, Gambardella A *et al*. 2009; A CREB-C/EBPbeta cascade induces M2 macrophage-specific gene expression and promotes muscle injury repair. *Proc Natl Acad Sci U S A* **106**: 17475–17480.

Sacks MS. 2000; Biaxial mechanical evaluation of planar biological materials. *J Elasticity* **61**: 199–246.

Sacks MS, Chuong CJ. 1992; Characterization of collagen fiber architecture in the canine diaphragmatic central tendon. *J Biomech Eng* **114**: 183–190.

Sanchez VM, Abi-Haidar YE, Itani KM. 2011; Mesh infection in ventral incisional hernia repair: incidence, contributing factors, and treatment. *Surg Infect (Larchmt)* **12**: 205–210.

Soletti L, Nieponice A, Hong Y *et al*. 2011; *In vivo* performance of a phospholipid-coated bioerodable elastomeric graft for small-diameter vascular applications. *J Biomed Mater Res A* **96**: 436–448.

Stankus JJ, Freytes DO, Badylak SF *et al*. 2008; Hybrid nanofibrous scaffolds from electrospinning of a synthetic biodegradable elastomer and urinary bladder matrix. *J Biomater Sci Polym Ed* **19**: 635–652.

Taniguchi S, Ueda K, Inoue T *et al*. 2006; Impact of collagen subtype proportions in peritoneal tissues on inguinal hernia formation in adults and infants. *Pediatr Surg Int* **22**: 600–604.

Ten Broek RW, Grefte S, Von den Hoff JW. 2010; Regulatory factors and cell populations involved in skeletal muscle regeneration. *J Cell Physiol* **224**: 7–16.

Tidball JG, Wehling-Henricks M. 2007; Macrophages promote muscle membrane repair and muscle fibre growth and regeneration during modified muscle loading in mice *in vivo*. *J Physiol* **578**: 327–336.

van der Linden FT, van Vroonhoven TJ. 1988; Long-term results after surgical correction of incisional hernia. *Neth J Surg* **40**: 127–129.

Wolf MT, Daly KA, Reing JE *et al*. 2012; Biologic scaffold composed of skeletal muscle extracellular matrix. *Biomaterials* **33**: 2916–2925.

Zhong T, Janis JE, Ahmad J *et al*. 2011; Outcomes after abdominal wall reconstruction using acellular dermal matrix: a systematic review. *J Plast Reconstr Aesthet Surg* **64**: 1562–1571.